Acta Cryst. (1977). A33, 548–553

Electron-Microscope and Diffraction Studies of Polytypism in Stilpnomelane

BY E. S. CRAWFORD, D. A. JEFFERSON AND J. M. THOMAS

Edward Davies Chemical Laboratories, University College of Wales, Aberystwyth SY23 1NE, Wales

(*Received* 20 *December* 1976; *accepted* 29 *January* 1977)

Several hitherto unreported, long-period polytypes of the complex layer silicate stilpnomelane have been identified by a combination of electron diffraction and high-resolution lattice-imaging techniques. The rich diversity of polytypes present in a Californian sample comprises two distinct 2-layer structures, one possessing triclinic, the other trigonal symmetry, a 3-layer trigonal variant, and further structures of, as yet, undetermined symmetry with 4, 5, 9 and 14 layers in the unit cell. Coherent intergrowths of the 9 and 14-layer polytypes have been observed in bright-field lattice images, and all polytypes show well-ordered electron-diffraction patterns. Specimens from this geological source, as well as two others (North Wales and New Zealand) display, in addition, disordered examples of the accepted, X-ray based, 1-layer triclinic structure. The fine details of the stacking arrangements (vector sequences) in the 2 and 3-layer polytypes have been determined from electron-diffraction data, and, from similarities in the variation of contrast with sample thickness in lattice images of 2 and 14-layer structures, it is possible to formulate a model for the structures of the longer-period polytypes.

1. Introduction

Polytypism in layer silicate minerals is a common phenomenon, its occurrence being almost inevitable in most of the known structures, owing to a distinctive feature in the construction of the individual structural layers. For example, in the mica family of minerals, for which the various polytypic modifications were originally discussed (Smith & Yoder, 1956), each layer consists of an octahedral component, built up of edge-sharing $M(O,OH)_6$ octahedra, flanked on either side by Si–O tetrahedral components. Owing to the geometry of the octahedra, the tetrahedral Si–O networks on either side of them cannot superimpose directly, but are displaced relative to one another. Consequently, if several different displacements are possible, distinct ordering schemes of displacement vectors in subsequent layers will produce different polytypes. Further possibilities of structural variation also exist: a 180° rotation of successive octahedral components may occur, thereby producing more displacement vectors. Moreover, if the layers contain ordered or disordered cation vacancies, or are linked by hydrogen bonds, yet a further set of different displacement vectors is introduced. Typical of this latter category are the kaolinite minerals (Bailey, 1963, 1969) cronstedtite (Steadman & Nuttall, 1963, 1964) and chlorite (Bailey & Brown, 1962; Brown & Bailey, 1963; Shirozu & Bailey, 1965).

Polytypism in layered silicates appears to differ in one important respect from the phenomenon exhibited by such materials as SiC and CdI_2, in that there is some evidence that the actual layer structure differs in detail according to the particular stacking sequence employed. Several structural analyses of mica polytypes (Radoslovich, 1959, 1960; Franzini, 1969; McCauley & Newnham, 1971) appear to confirm this, and also suggest that slight structural changes can be accompanied by cationic substitution (Levinson, 1953; Takeda & Burnham, 1969). Layered silicates showing a stacking disorder, interpreted as microfine intergrowths of different polytypes, are also common, and in zussmanite, a definite correlation between the degree of disorder and the amount of cationic substitution has been established (Jefferson, 1976).

Systems exhibiting polytypism have traditionally been investigated by single-crystal X-ray diffraction methods, but these tend to be impracticable when applied to fine-grained silicates of the kind discussed here, and electron diffraction, though it suffers from limitations imposed by multiple scattering, is, as we demonstrate below, useful. Furthermore, when applied to disordered systems, X-ray diffraction methods yield only an 'average Patterson function' (Cochran & Howells, 1954) which, although interpretable for simple structures (Jefferson & Bown, 1974), becomes exceedingly complex when several displacement vectors are operative. Electron diffraction, however, can be readily combined with high-resolution lattice imaging techniques, which have recently been used to reveal disorder directly in several oxide and silicate systems (Iijima & Buseck, 1975; Hutchison, Irusteta & Whittaker, 1975; Nakajima, Morimoto & Watanabe, 1975). We now discuss how this combination of techniques has proved helpful in elucidating the ultrastructural characteristics of stilpnomelane [idealized formula $K_2Fe_{48}Si_{70}Al_2O_{180}(OH)_{48}$].

2. Structure

The structure of stilpnomelane deduced from X-ray studies by Eggleton (1972), henceforth referred to as the Eggleton structure, bears some resemblance to that of zussmanite (Lopes-Vieira & Zussman, 1969) in that the Si–O components of the layers are not an infinite,

two-dimensional network of six-membered rings of SiO_4 tetrahedra, but consist of distinct 'islands' or 'rafts'. These islands (Fig. 1) comprise seven six-membered rings of tetrahedra, and are linked by other six-membered rings, the latter having only trigonal symmetry. These latter rings are also bonded to their counterparts on adjacent layers, hence the layers are linked by Si–O bonds, so that intercalation is not expected or observed. The complexity of the structure when compared with that of mica is shown by the large a dimension of 21·1 Å ($a = 5{\cdot}4$ Å for mica), and although the repeat unit in the plane of the layers has a hexagonal shape the overall symmetry of the Eggleton structure is triclinic, with an interlayer spacing of 12·2 Å.

In stilpnomelane 48 different displacement vectors of any one layer with respect to its predecessor exist, the same as the number of octahedra within the hexagonal unit mesh (Fig. 2). As the layers, considered independently, possess trigonal symmetry, these 48 alternatives may be grouped into 16 triplets, of which the group $(\mathbf{V}_{11},\mathbf{V}_{15},\mathbf{V}_{20})$ was suggested by Eggleton as a possibility for the determined structure, or $(\mathbf{V}_{26},\mathbf{V}_{30},\mathbf{V}_{34})$ for its twin-related form. These, and the majority of the triplets, produce triclinic $P\bar{1}$ structures, but there are four $(\mathbf{V}_1,\mathbf{V}_{41},\mathbf{V}_{48})$. $(\mathbf{V}_5,\mathbf{V}_{40},\mathbf{V}_{45})$, $(\mathbf{V}_{14},\mathbf{V}_{29},\mathbf{V}_{47})$ and $(\mathbf{V}_{17},\mathbf{V}_{46},\mathbf{V}_{47})$ which would produce $C2/m$ monoclinic polytypes. In stilpnomelane, unlike zussmanite, there is no single displacement vector which, if repeated regularly, will produce a rhombohedral structure, and the two groups of vectors proposed by Eggleton come as near to this as the structure will permit. In addition to the 48 displacement vectors illustrated in Fig. 2, a further set of 48 is available if 180° rotation of successive octahedral components occurs, the latter being obviously related to the vectors of Fig. 2 by inversion through the repeat unit origin.

Fig. 3 illustrates idealized reciprocal lattice sections of stilpnomelane for the Eggleton structure. In common with that of many layered silicates the reciprocal

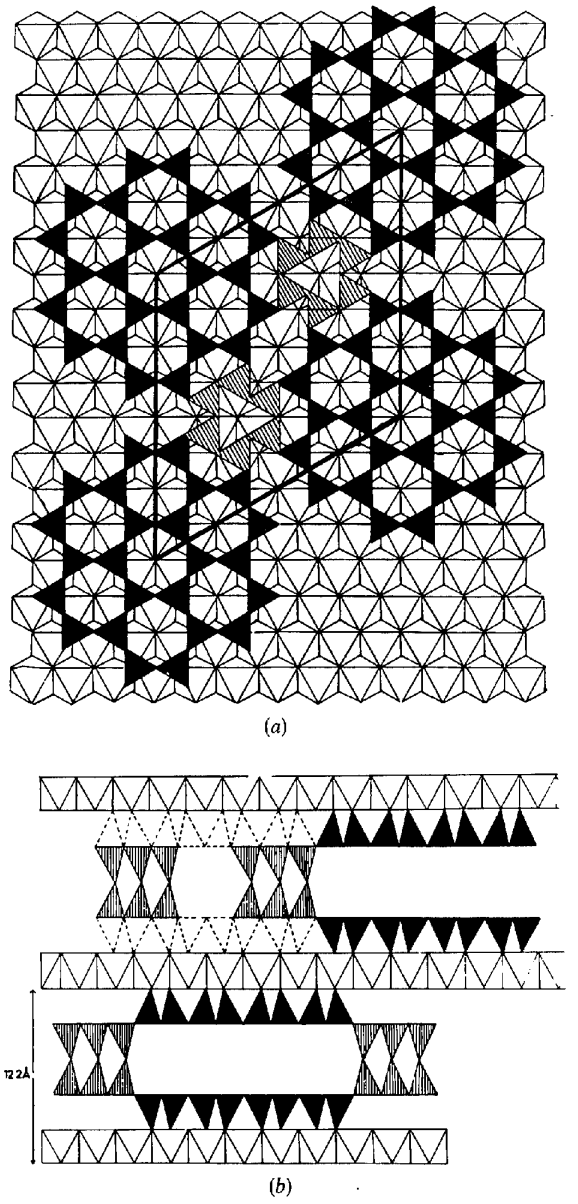

Fig. 1. The stilpnomelane structure projected on (*a*) (001) (*b*) down [010]. Tetrahedra comprising 'rafts' or 'islands' are shown solid – linking tetrahedra are shaded.

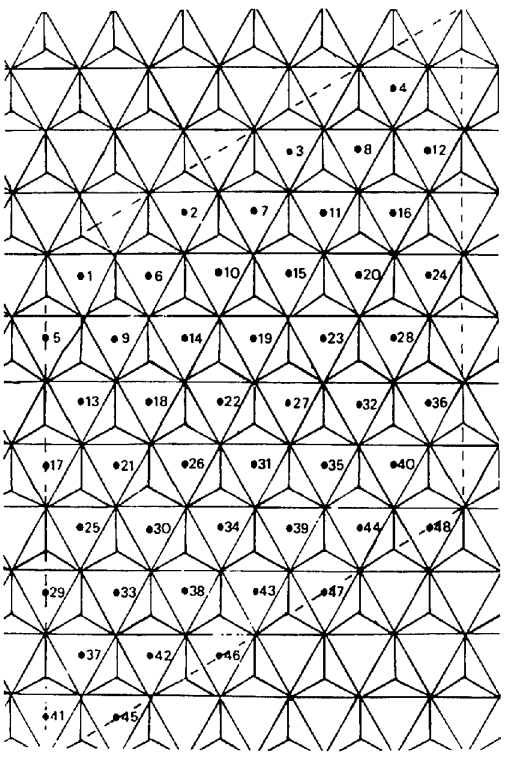

Fig. 2. Nomenclature of possible displacement vectors in the stilpnomelane structure (see text). Each numbered position represents a possible origin for the next layer.

lattice of stilpnomelane contains certain rows of spots parallel to **z*** which are much stronger than average, and tend to be relatively unaffected by the presence of a stacking disorder, which streaks out the other rows parallel to **z***. Such strong rows correspond to a hexagonal sub-cell, with X and Y axes parallel to and equal in magnitude to the edges of the octahedra. Recent theoretical considerations (Jefferson, 1977) of stacking disorders in materials such as stilpnomelane have shown that, whereas other rows are streaked parallel to **z*** by all types of stacking displacement, the strong, 'sub-cell' rows are affected only if rotation of successive octahedral components also occurs. Even when this condition is met, certain 'sub-cell' rows, *i.e.* those with *sub-cell* indices such that $2h+k=3n$, are still unaffected, in an exactly analogous manner as that shown in systems possessing c.c.p./h.c.p. stacking disorders. Experimental evidence has also been obtained to indicate that, in certain samples of stilpnomelane, octahedral rotations do occur, a phenomenon which is relatively rare in layered silicates.

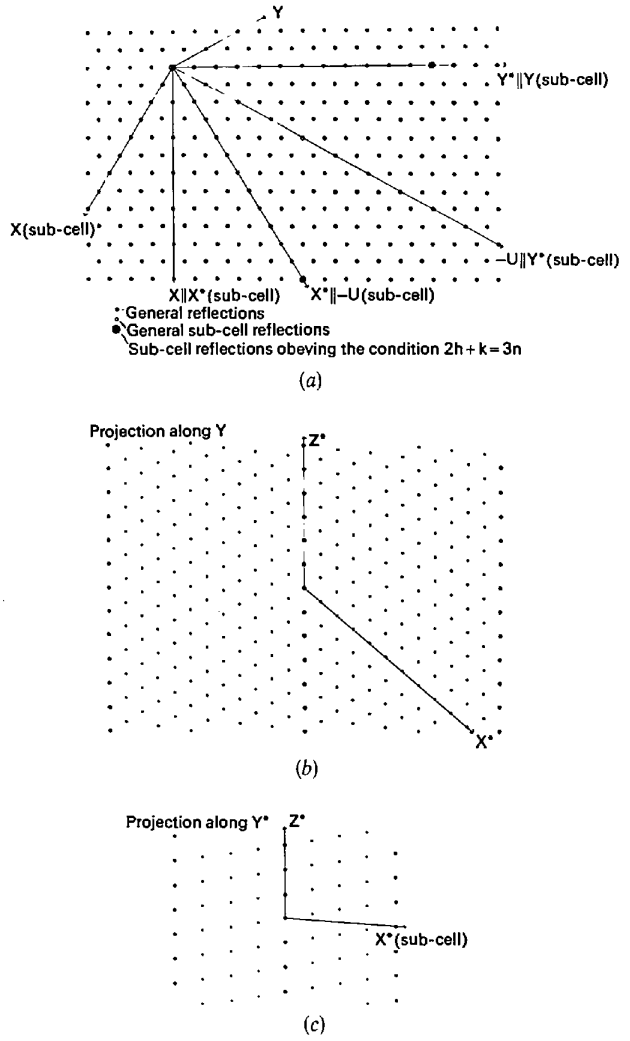

Fig. 3. Idealized reciprocal lattice for one of the six Eggleton structures. (*a*) Projection down **z***, (*b*) ($h0l$) section, (*c*) ($2h,\bar{h},l$) section.

3. Experimental

Three samples of stilpnomelane were examined, these originating from the Laytonville district, California (A2018), Otago, New Zealand (A2019), and Rhyd, North Wales (A2079). Crushed powder specimens deposited on holey carbon films yielded only reciprocal-lattice projections of the type shown in Fig. 3(*a*), the stilpnomelane flakes, unlike those of montmorillonite (Suito, Arakawa & Yoshida, 1969), being too brittle to curl up at the edges and reveal the layer stacking arrangement, and were rejected in favour of ion-thinned specimens prepared from resin-impregnated petrological sections (Phakey, Curtiss & Oertel, 1972) which gave, with suitable tilting, reciprocal lattice sections containing the **z*** axis. Specimens were examined in a Philips EM300 electron microscope with a eucentric goniometer stage, and a Siemens Elmiskop 102A fitted with a double-tilt stage. An image intensification system attached to the EM300 greatly facilitated image recording. Contrast in lattice images was generally poor, the absence of any potential 'tunnels' similar to those in beryl (Buseck & Iijima, 1974) making a PCD interpretation (Lynch, Moodie & O'Keefe, 1975) somewhat difficult. For the characterization of displacement disorders, however, simple fringe images appear to be adequate (Jefferson & Thomas, 1975), and consequently the focus of the objective lens was adjusted to obtain merely optimum contrast for one set of $00l$ and $hk0$ or $0kl$ fringes, which thereby gave a simple, two-dimensional image. Electron-diffraction patterns for the various polytypes were compared with calculated intensity distributions for the various structural possibilities, the effects of layer form factor and multiple scattering being neglected. As the influence of the latter can be considered as a repeated self-convolution of a set of diffracted amplitudes (Cowley & Moodie, 1957), its effect is to mask any characteristic intensity variations in the diffraction pattern. Consequently, the mere presence of such variations guarantees their authenticity. The effect of multiple scattering upon image contrast, however, appears to be much more critical, and will be discussed below in the context of image interpretation, as with specimen thickness of some 200–500 Å the effects were considerable.

4. Results

As regards the abundance of polytypic modifications, the Californian sample (A2018) was by far the most interesting; consequently, the other two samples will be discussed only briefly. Selected-area electron-diffraction patterns from A2018 showed a variety of arrangements (Fig. 4). Fig. 4(*a*) and (*b*) were characteristic of the Eggleton structure occurring alone, and in its

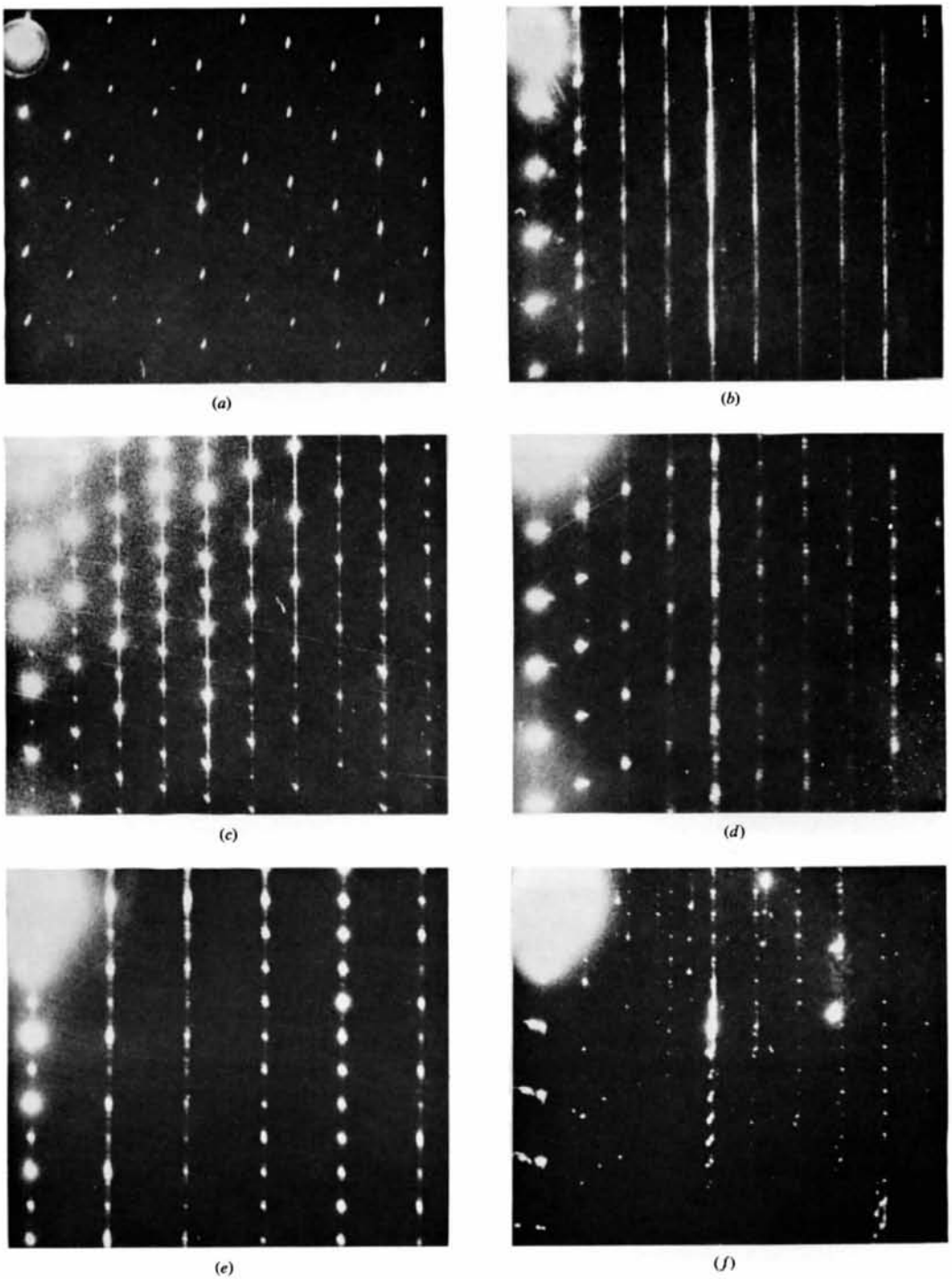

Fig. 4. Selected-area electron diffraction patterns from the Californian sample (*a*) Eggleton structure, (*h*0*l*) section, (*b*) as (*a*), but in twin form, (*h*0*l*) section, (*c*) 2-layer triclinic structure, (*h*0*l*) section, (*d*) 2-layer triclinic structure, (0*kl*) section, (*e*) 2-layer trigonal structure, ($2h,\bar{h},l$) section, (*f*) 3-layer trigonal structure, (*h*0*l*) section.

[*To face p.* 550

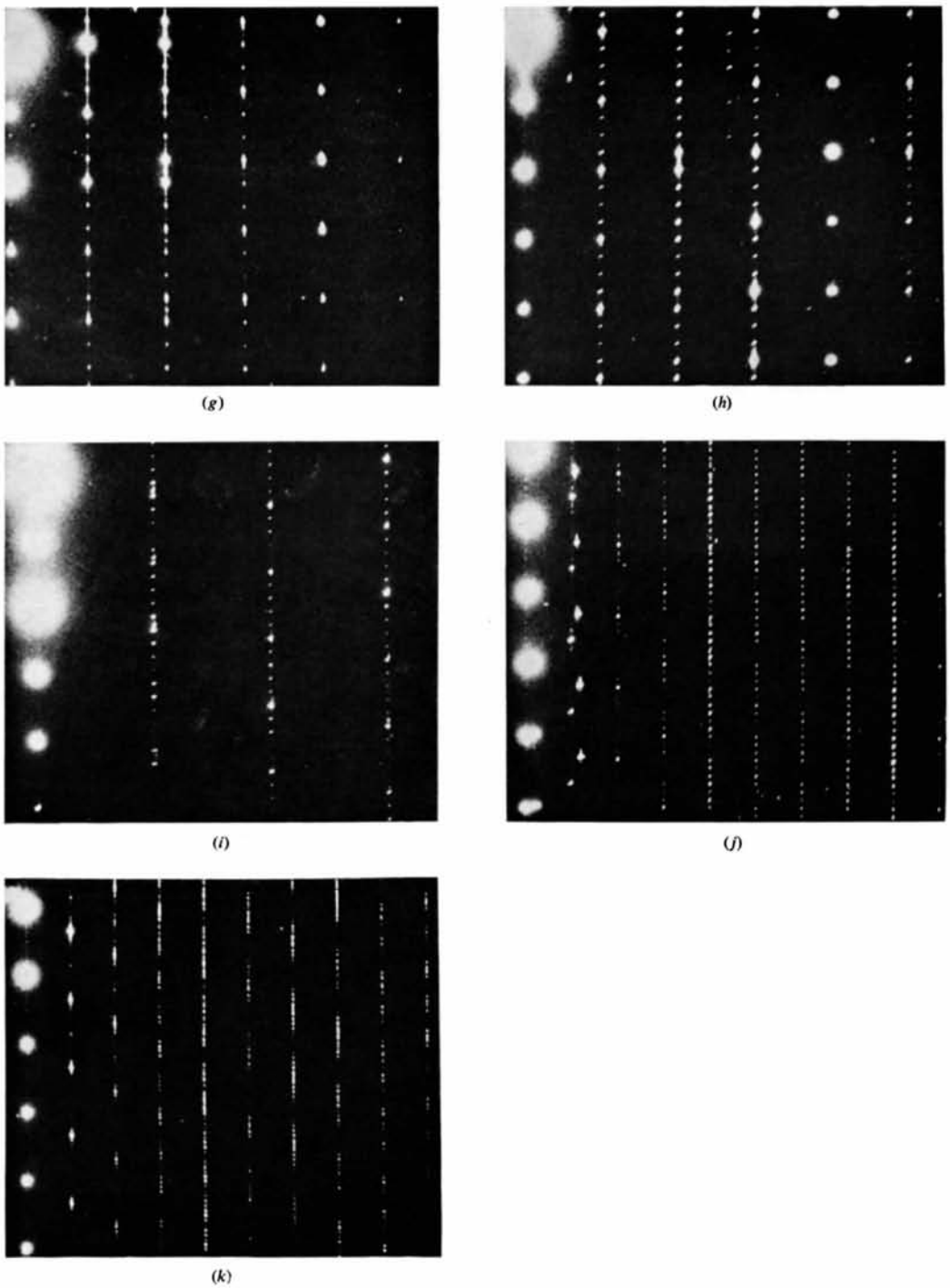

Fig. 4. (*cont.*) (*g*) 3-layer trigonal structure $(2h,\bar{h},l)$ section, (*h*) 4-layer structure, $(2h,\bar{h},l)$ section, (*i*) 5-layer structure, $(3h,\bar{h},l)$ section, (*j*) 9-layer structure, (*h*0*l*) section, (*k*) 4-layer structure, (*h*0*l*) section. (The symmetries of the last four structures remain to be determined.)

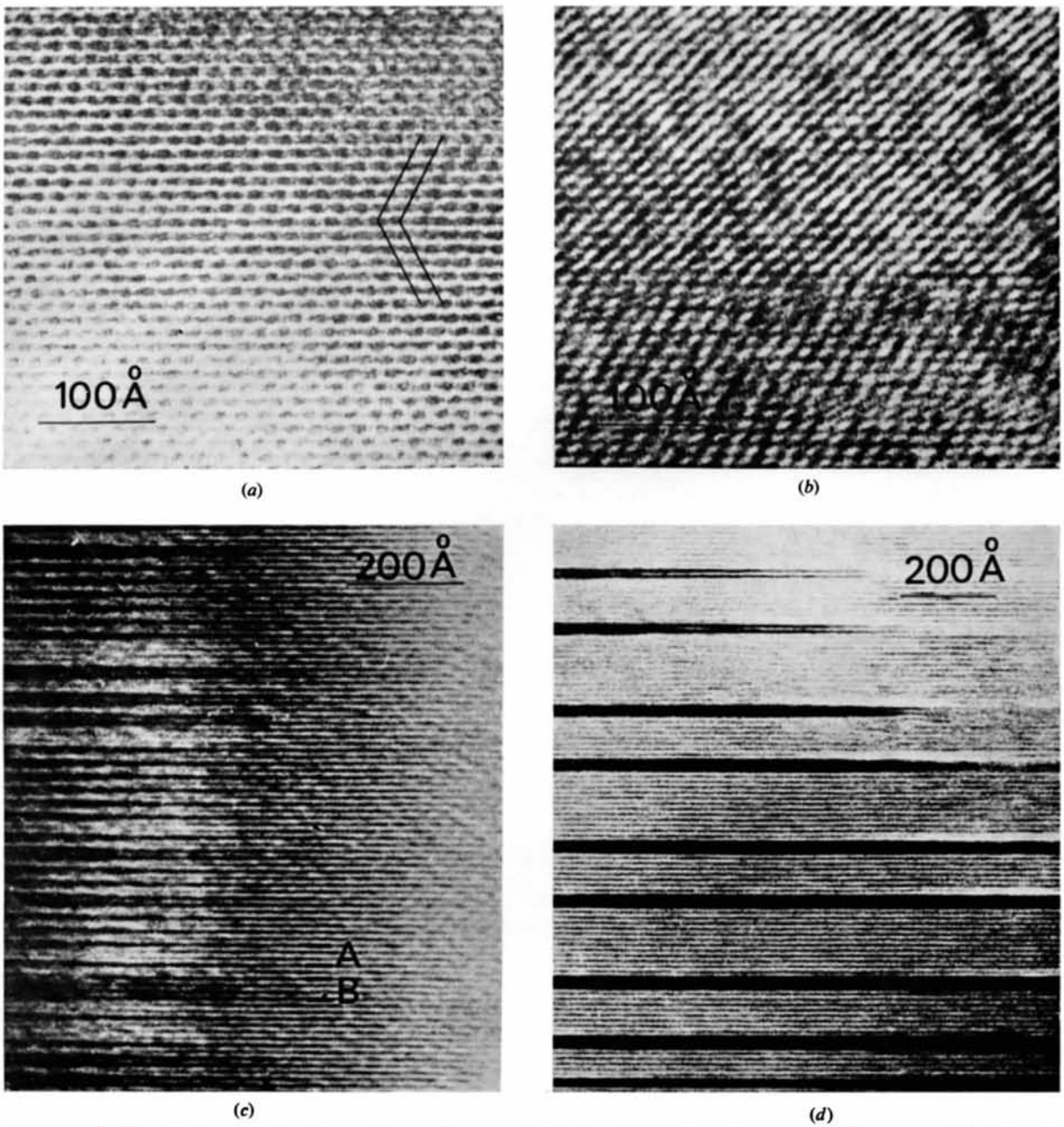

Fig. 5. Bright-field lattice images of stilpnomelane polytypes. (*a*) Twinned Eggleton structure. (*b*) Intergrown Eggleton structures. (*c*) Disordered 2-layer trigonal structure with regions of 1, 3 and 4-layer polytypes indicated. (*d*) Coherent intergrowth of 9 and 4-layer polytypes.

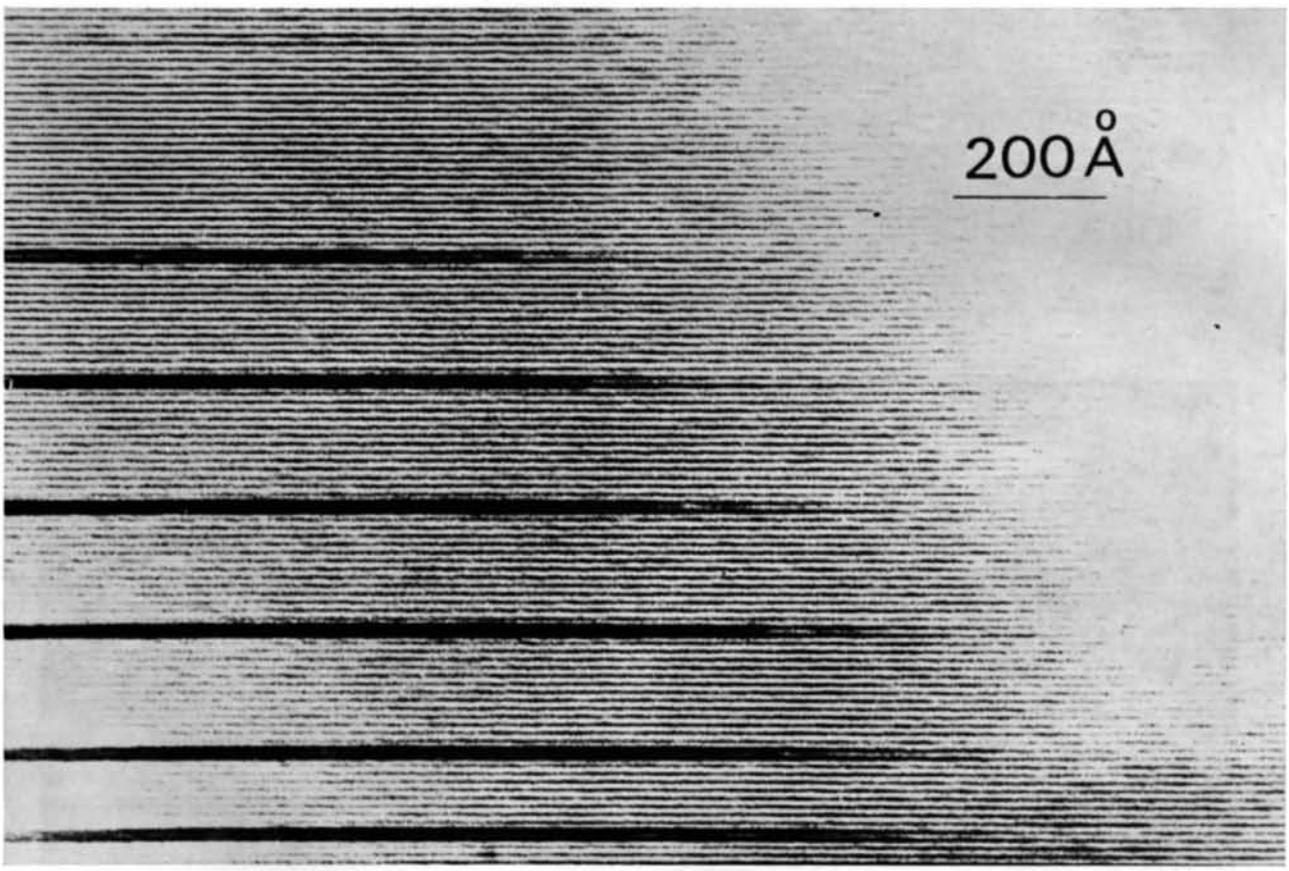

Fig. 6. A micrograph of the same sample as Fig. 5 (*d*), illustrating the crystal edge with the true periodicity of the longer-period polytypes becoming apparent as the thickness increases.

twinned form, as expected, but three distinct patterns corresponding to 2-layer structures were observed. Fig. 4(*c*) illustrates a simple 2-layer reciprocal lattice with oblique mesh, but that in Fig. 4(*d*) is more complex, again with an oblique mesh, but with an intensity variation such that rows with l odd had intensity maxima rising from zero to a maximum as k varied from 0 to 12, rows with l even showing the opposite behaviour. Fig. 4(*e*) illustrates a third type, with a rectangular mesh, and sub-cell rows of spots showing a doubled periodicity indicative of octahedral rotation. In all cases considerable disorder, indicated by streaking parallel to $\mathbf{z}^*$, was present. In an exactly analogous manner to Fig. 4(*c*) and (*d*), Fig. 4(*f*) and (*g*) indicate three-layer arrangements with rectangular meshes, the former having a simple pattern, and the latter showing pronounced intensity variations, $l=3n$ reflexions having maxima at $h=0$ and zero at $h=4$ and 8, whereas with $l=3n+1$ and $l=3n-1$ the maxima were shifted to $h=4$ and $h=8$ respectively. More complex polytypes were also revealed, Fig. 4(*h*) and (*i*) showing 4 and 5-layer arrangements respectively, both with oblique lattice meshes. The most complex patterns, however, are shown by Fig. 4(*j*) and (*k*), these indicating 9 and 14-layer polytypes respectively, the latter with an apparently rectangular lattice mesh. In both cases, the degree of long-range order was reasonably high, although some lattice images (discussed below) revealed coherent intergrowths between the 9 and 14-layer structures. In comparison with the Californian sample, the samples from Otago and Rhyd only showed evidence for the Eggleton structure, either as almost perfect crystals, or with a disorder so severe that no structure type could be assigned.

Lattice images of the Californian sample are illustrated in Fig. 5. The images were, in general, of two types. In favourable circumstances, when very thin regions could be examined, true two-dimensional images were obtained so that the stacking sequence could be observed directly. In most cases, however, specimens appeared to be too thick to provide observable contrast for $h0l$ or $0kl$-type fringes, and the images could no longer be considered as being within the limits of the PCD approximation. The existence of multiple scattering in such specimens was demonstrated by the diffraction patterns, where systematic absences on the $00l$ reciprocal-lattice row were not, in general, observed. Consequently, interpretation of structural features in these images was not possible without recourse to N-beam dynamical calculations (Allpress, Hewat, Moodie & Sanders, 1972), which are at present being undertaken, and only the overall periodicity of the structures shown can be regarded as reliable. The superlattice, however, is accentuated by multiple scattering, a feature which has been noted in certain ferrites (Van Landuyt, Amelinckx, Kohn & Eckart, 1974).

Of the various lattice images obtained, those typified in Fig. 5(*a*) and (*b*) were by far the most common; Fig. 5(*a*) shows a two-dimensional image of the twinned version of the Eggleton structure, whereas Fig. 5(*b*) indicates two similar, but distinct, Eggleton structures, utilizing the vectors $\mathbf{V}_{11}$ and $\mathbf{V}_{30}$ respectively. In such images, the vectors operating in regions of the different polytypes were obtained by measurement of the angles between $h0l$ and $00l$-type fringes, a procedure which, unfortunately, failed to give completely unambiguous results except when images could be obtained with the electron beam parallel to both $\mathbf{x}$ and $\mathbf{x}^*$. This, however, was not generally possible. It was therefore assumed that, in general, only the six vectors described by Eggleton were present, this being supported by evidence from the longer-period polytypes, discussed below. Images of the multiple-layer polytypes were generally of the form shown in Fig. 5(*c*), which shows principally a 2-layer polytype [corresponding to the diffraction pattern of Fig. 4(*e*)]. Although the image appears to be of an essentially one-dimensional type, sufficient information from rows other than $00l$ (which should, in the absence of multiple scattering, be identical for all polytypes) is incorporated into the image to indicate the overall 2-layer periodicity and to highlight various regions where the local periodicity appears to be 1, 3, and even 4 layers. With an image of this type, the principal difficulty is to distinguish between, say, on the one hand, a 4-layer polytype inserted into a 2-layer polytype host, and, on the other hand, four layers of a 1-layer polytype inserted into the same host; but a definite distinction exists in the image, as shown by the regions *A* and *B*. In this case, owing to a similarity of contrast between region *A* and the basic, 2-layer structure, the former was considered to be a true, 3-layer sequence, region *B* being three layers of the 1-layer polytype. A similar problem exists in the image of Fig. 5(*d*), which shows an intergrowth of mainly 14 and 9-layer polytypes, although 5, 7 and 20-layer sequences are also indicated. In this case, however, sufficient evidence was visible in the diffraction pattern to confirm the main polytypes present. Moreover, in certain areas extending over a region of *ca* 1000 Å, ordered intergrowth of the 14 and 9-layer structures was clearly visible. In none of the images of the longer-period polytypes, however, was it possible to determine the stacking sequence directly.

5. Discussion

The existence of so many, hitherto unreported, polytypes of the stilpnomelane structure is surprising in view of their relatively well-ordered nature, when compared with the severely disordered picture revealed in previous X-ray studies (Smith & Frondel, 1968; Eggleton, 1972). Owing to the extremely large number of polytypic modifications possible even for only 1 or 2-layer structures, no attempt was made to elucidate the structures of the longer-period phases, and structural analysis was concentrated on the 2 and 3-layer modifications, where intensity variations in reciprocal

space were sufficiently distinct to be relatively unaffected by multiple scattering. Although lattice images of the 1-layer structures could not conclusively eliminate the presence of vectors other than the six proposed by Eggleton, no direct evidence was obtained to suggest that any others were operative. Hence, in the initial calculations it was assumed that only these six, $(\mathbf{V}_{11}, \mathbf{V}_{15}, \mathbf{V}_{20})$ and $(\mathbf{V}_{26}, \mathbf{V}_{30}, \mathbf{V}_{34})$, were possible. Measurement of the oblique mesh of Fig. 4(*d*) indicated that it could result from any combination of two of these vectors from the same group. Consequently, each of the six combinations possible was used to calculate theoretical diffracted intensities, and for each it was found that one of the three principal reciprocal-lattice sections [*i.e.* (*h*0*l*), (0*kl*) or ($h\bar{h}l$)] showed an intensity variation which corresponded to that of Fig. 4(*d*). In addition, for each combination, one principal section was found to correspond to Fig. 4(*d*) and one to Fig. 4(*c*), demonstrating that both patterns were characteristic of a single, 2-layer triclinic polytype. When all possible vectors were included in the calculation, no other combination gave agreement with both Fig. 4(*c*) and (*d*), and it was therefore concluded that only the vectors listed above were involved.

Similar analysis was applied to the 3-layer patterns illustrated in Fig. 4(*f*) and (*g*). In this case, however, only the two combinations $\mathbf{V}_{11}+\mathbf{V}_{15}+\mathbf{V}_{20}$ and $\mathbf{V}_{26}+\mathbf{V}_{30}+\mathbf{V}_{34}$ were considered, as they alone would produce an orthogonal cell. Both combinations produced good agreement with the ($2h,\bar{h},l$) type reciprocal-lattice sections of Fig. 4(*g*), while the (*h*0*l*)-type calculated sections also agreed with those observed in Fig. 4(*f*). Accordingly, as with the 2-layer polytype, both the patterns of Fig. 4(*f*) and (*g*) were assigned to a single, 3-layer polytype. In this case, however, the overall symmetry was trigonal. The remaining simple polytype observed was that giving rise to the diffraction pattern of Fig. 4(*e*). Overall symmetry was again trigonal, although the structure was only of a 2-layer variety, but with 180° rotation of successive octahedral components. Unlike the previously described 2 and 3-layer polytypes, the diffraction pattern of Fig. 4(*e*) showed no pronounced intensity variations, and consequently its structure could not be determined uniquely. However, in the light of the 2 and 3-layer structures described above, it would seem likely that this 2-layer trigonal form would also employ one of the six vectors proposed by Eggleton.

The structures of the remaining polytypes have not yet been elucidated, mainly owing to insufficiently strong diffracted intensity variations, which makes testing of various models somewhat inconclusive. However, some structural conclusions may be drawn from a comparison of bright-field images of the more complicated polytypes with the simpler, 2-layer trigonal form. In the images of the latter, a distinctive feature is the manner in which the 2-layer repeat becomes apparent as the crystal thickness increases (*i.e.* as the distance from the edge of the wedge-shaped specimen increases). This contrast effect would therefore appear to be associated with the rotation of successive octahedral components. In images of the more complex polytypes, similar effects were noted (Fig. 6) near the edge of the specimen. Such structures could therefore be built up of blocks of one of the simpler polytypes, the blocks being bounded by *pairs* of layers, with octahedral rotation occurring within the latter, but not in the blocks themselves. Investigations of the validity of this model are in progress, but explanation of this image contrast requires full *N*-beam dynamical calculations, which as yet, are not available for stilpnomelane.

The origins of polytypism in stilpnomelane remain obscure. However, it does seem probable that these structures arise from some form of ordering scheme in what is usually a very severely disordered mineral, where usually randomly arranged displacement vectors are forced into a more regular disposition by an outside influence. This is supported by the fact that the Californian sample proved to have the greatest variety of polytypes, this sample coming from a geological area noted for mineral formation at extremely high pressure. However, the opportunity for chemical substitution to give rise to ordered polytypes also exists, and in view of evidence obtained for such processes in zussmanite (Jefferson, 1976), which comes from the same region, this remains a strong possibility.

The authors thank Dr J. L. Hutchison and Professor J. S. Anderson for the opportunity to use the Siemens Elmiskop 102A electron microscope, and Dr D. A. Jenkins, Department of Soil Science, UCNW, Bangor, for providing the stilpnomelane samples from Rhyd. The Philips EM300 was provided by the Science Research Council, and one of us (ESC) was in receipt of a University College of Wales research studentship which is gratefully acknowledged.

References

ALLPRESS, J. G., HEWATT, E. A., MOODIE, A. F. & SANDERS, J. V. (1972). *Acta Cryst.* A**28**, 528–536.
BAILEY, S. W. (1963). *Amer. Min.* **48**, 1196–1209.
BAILEY, S. W. (1969). *Clays Clay Min.* **17**, 355–371.
BAILEY, S. W. & BROWN, B. E. (1962). *Amer. Min.* **47**, 819–850.
BROWN, B. E. & BAILEY, S. W. (1963). *Amer. Min.* **48**, 42–61.
BUSECK, P. R. & IIJIMA, S. (1974). *Amer. Min.* **59**, 1–21.
COCHRAN, W. & HOWELLS, E. R. (1954). *Acta Cryst.* **7**, 412–415.
COWLEY, J. M. & MOODIE, A. F. (1957). *Acta Cryst.* **10**, 609–619.
EGGLETON, R. A. (1972). *Miner. Mag.* **38**, 693–711.
FRANZINI, M. (1969). *Contr. Miner. Petrol.* **21**, 203–224.
HUTCHISON, J. L., IRUSTETA, M. C. & WHITTAKER, E. J. W. (1975). *Acta Cryst.* A**31**, 794–801.
IIJIMA, S. & BUSECK, P. R. (1975). *Amer. Min.* **60**, 758–770.
JEFFERSON, D. A. (1976). *Amer. Min.* **61**, 470–483.
JEFFERSON, D. A. (1977). In preparation.
JEFFERSON, D. A. & BOWN, M. G. (1974). *Nature, Phys. Sci.*, **245**, 43–44.

JEFFERSON, D. A. & THOMAS, J. M. (1975). *Mater. Res. Bull.* **10**, 761–768.
LEVINSON, A. A. (1953). *Amer. Min.* **38**, 88–107.
LOPES-VIEIRA, A. & ZUSSMAN, J. (1969). *Miner. Mag.* **37**, 49–60.
LYNCH, D. F., MOODIE, A. F. & O'KEEFE, M. A. (1975). *Acta Cryst.* A**31**, 300–307.
MCCAULEY, J. W. & NEWNHAM, R. E. (1971). *Amer. Min.* **56**, 1626–1637.
NAKAJIMA, Y., MORIMOTO, N. & WATANABE, E. (1975). *Proc. Japan Acad.* **51**, 173–178.
PHAKEY, P. P., CURTISS, C. D. & OERTEL, G. (1972). *Clays Clay Min.* **20**, 193–197.
RADOSLOVICH, E. W. (1959). *Nature, Lond.* **183**, 253.
RADOSLOVICH, E. W. (1960). *Acta Cryst.* **13**, 919–932.
SHIROZU, H. & BAILEY, S. W. (1965). *Amer. Min.* **50**, 868–885.
SMITH, J. V. & YODER, H. S. (1956). *Miner. Mag.* **31**, 209–235.
SMITH, M. L. & FRONDEL, C. (1968). *Miner. Mag.* **36**, 893–913.
STEADMAN, R. & NUTTALL, P. M. (1963). *Acta Cryst.* **16**, 1–8.
STEADMAN, R. & NUTTALL, P. M. (1964). *Acta Cryst.* **17**, 404–407.
SUITO, E., ARAKAWA, M. & YOSHIDA, T. (1969). *Proc. Int. Clay Conf. Tokyo*, **1**, 757.
TAKEDA, H. & BURNHAM, C. W. (1969). *Miner. J. Japan*, **6**, 102–109.
VAN LANDUYT, J., AMELINCKX, S., KOHN, J. A. & ECKART, D. W. (1974). *J. Solid State Chem.* **9**, 103–119.

Acta Cryst. (1977). A**33**, 553–555

A Sequence of Nested Neighborhoods of the Structure Invariant $\varphi_{\mathbf{h}}+\varphi_{\mathbf{k}}+\varphi_{\mathbf{l}}+\varphi_{\mathbf{m}}$

BY HERBERT HAUPTMAN

Medical Foundation of Buffalo, 73 High Street, Buffalo, New York 14203, *USA*

(*Received* 14 *June* 1976; *accepted* 21 *January* 1977)

A sequence of nested neighborhoods of the structure invariant $\varphi=\varphi_{\mathbf{h}}+\varphi_{\mathbf{k}}+\varphi_{\mathbf{l}}+\varphi_{\mathbf{m}}$ is derived. Each neighborhood is a subset of the succeeding ones and consists of the small number of structure factor magnitudes $|E|$ upon which, in favorable cases, the value of φ mostly depends. Thus the stage is set for deriving reliable estimates for φ in terms of known magnitudes $|E|$ *via* appropriate conditional probability distributions.

1. Introduction

In recent work on the theory of the structure invariants and seminvariants (Hauptman, 1975*a*,*b*) a novel probabilistic background was formulated and mathematical methods introduced in order to obtain a new class of probability distributions. These lead to estimates of the structure invariants and seminvariants φ which are particularly good in the favorable case that the variance of the distribution happens to be small. The major result was that the value of φ is mostly determined by one or more appropriately chosen small sets of structure factor magnitudes $|E|$, the neighborhoods of φ, and is relatively insensitive to the values of the great bulk of the remaining magnitudes. In particular, a principle of nested neighborhoods was formulated which posits the existence of one or more sequences of nested neighborhoods of φ, each neighborhood a subset of the succeeding one, with the property that φ may be estimated in terms of the magnitudes $|E|$ constituting any neighborhood (or a suitable subset) of φ and that the more magnitudes in the neighborhood the better the estimate 'in the probabilistic sense', *i.e.* with more magnitudes there is a greater potential for obtaining a distribution with a small variance.

More recently (Hauptman, 1976), the identity of the first two neighborhoods of each of the structure seminvariants φ, $\varphi_1+\varphi_2$, $\varphi_1+\varphi_2+\varphi_3$, $\varphi_1+\varphi_2+\varphi_3+\varphi_4$ in the space group $P\bar{1}$ was determined and, for some of these neighborhoods, the associated conditional probability distribution of the structure seminvariant derived (Green & Hauptman, 1976, 1977; Hauptman & Green, 1977). This preliminary work confirms the importance of the neighborhood concept, and its central role in future developments now seems assured. In view of the earlier work it appears likely too that the problem of deriving the conditional probability distribution of a structure invariant or seminvariant, given an arbitrary set of magnitudes $|E|$, will present no insuperable obstacle, although the analysis may be long and tedious. There remains therefore first the problem of identifying a suitable sequence of nested neighborhoods for a given structure invariant or seminvariant. The present paper is devoted to the solution of this problem for the four-phase structure invariant (quartet)

$$\varphi=\varphi_{\mathbf{h}}+\varphi_{\mathbf{k}}+\varphi_{\mathbf{l}}+\varphi_{\mathbf{m}} \tag{1.1}$$

where

$$\mathbf{h}+\mathbf{k}+\mathbf{l}+\mathbf{m}=0\,. \tag{1.2}$$

In the accompanying papers (Hauptman, 1977*a*,*b*) the related probability distributions in $P1$ and $P\bar{1}$ are derived and, in subsequent papers, the importance of these distributions in the applications will be demonstrated.